Nanoscale

Accepted Manuscript

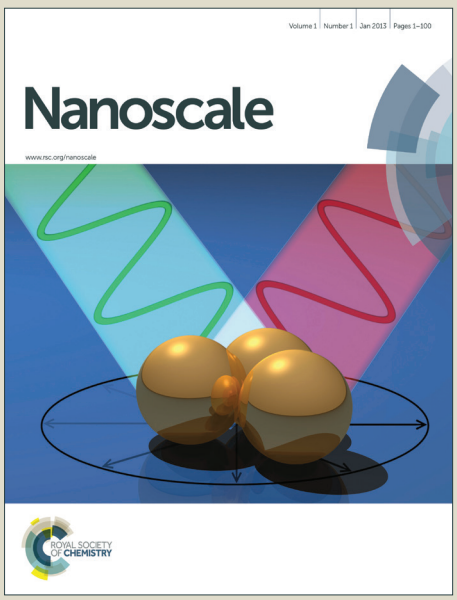

This is an *Accepted Manuscript*, which has been through the Royal Society of Chemistry peer review process and has been accepted for publication.

Accepted Manuscripts are published online shortly after acceptance, before technical editing, formatting and proof reading. Using this free service, authors can make their results available to the community, in citable form, before we publish the edited article. We will replace this *Accepted Manuscript* with the edited and formatted *Advance Article* as soon as it is available.

You can find more information about *Accepted Manuscripts* in the Information for Authors.

Please note that technical editing may introduce minor changes to the text and/or graphics, which may alter content. The journal's standard Terms & Conditions and the Ethical guidelines still apply. In no event shall the Royal Society of Chemistry be held responsible for any errors or omissions in this *Accepted Manuscript* or any consequences arising from the use of any information it contains.

ROYAL SOCIETY OF CHEMISTRY

www.rsc.org/nanoscale

Influence of the Glycocalyx and Plasma Membrane Composition on Amphiphilic Gold Nanoparticle Association with Erythrocytes

Prabhani U. Atukorale,[a] Yu Sang S. Yang,[b] Ahmet Bekdemir,[c] Randy P. Carney,[c] Paulo J. Silva,[c] Nicki Watson,[d] Francesco Stellacci,[c] & Darrell J. Irvine* [a b e f g h]

Authors' Affiliations:

* Corresponding author

[a] Department of Biological Engineering, [b] Department of Materials Science and Engineering, [e] Institute for Soldier Nanotechnologies, & [f] Koch Institute for Integrative Cancer Research, Massachusetts Institute of Technology, Cambridge, Massachusetts 01239, United States

[c] Institute of Materials, Ecole Polytechnique Federale de Laussane, 1015 Lausanne, Switzerland

[d] Whitehead Institute for Biomedical Research, Cambridge, Massachusetts 01239, United States

[g] Ragon Institute of MGH, MIT, and Harvard, Cambridge, Massachusetts 02139, United States

[h] Howard Hughes Medical Institute, Chevy Chase, Maryland 20815, United States

Nanoscale Accepted Manuscript

Abstract

Erythrocytes are attractive as potential cell-based drug carriers because of their abundance and long lifespan *in vivo*. Existing methods for loading drug cargos into erythrocytes include hypotonic treatments, electroporation, and covalent attachment onto the membrane, all of which require *ex vivo* manipulation. Here, we characterized the properties of amphiphilic gold nanoparticles (amph-AuNPs), comprised of a ~2.3 nm gold core and an amphiphilic ligand shell, which are able to embed spontaneously within erythrocyte membranes and might provide a means to load drugs into red blood cells (RBCs) directly *in vivo*. Particle interaction with RBC membranes occurred rapidly at physiological temperature. We further show that amph-AuNP uptake by RBCs was limited by the glycocalyx and was particularly influenced by sialic acids on cell surface proteoglycans. Using a reductionist model membrane system with synthetic lipid vesicles, we confirmed the importance of membrane fluidity and the glycocalyx in regulating amph-AuNP/membrane interactions. These results thus provide evidence for the interaction of amph-AuNPs with erythrocyte membranes and identify key membrane components that govern this interaction, providing a framework for the development of amph-AuNP-carrying erythrocyte 'pharmacytes' *in vivo*.

Key words: amphiphilic gold nanoparticles, erythrocytes, glycocalyx, plasma membrane, passive nanoparticle-membrane interaction, model membranes

Nanoscale Accepted Manuscript

Introduction

Targeting erythrocytes (red blood cells, or RBCs) as cellular carriers of therapeutic drug molecules has been of interest for many years. Erythrocytes are highly attractive as potential 'pharmacytes' for several key reasons.[1,2] They are the most abundant cells in the body and are readily available; humans have ~2.5 x 10^{13} erythrocytes, produced constantly at a rate of 2 million cells per second. They have a long ~120-day lifespan in circulation, and this feature can be exploited in applications where slow and sustained cargo release into the intravenous circulation is desired. For example, erythrocytes have been used as circulating depots of vitamins[3] and steroids[4–7], agents for antineoplastic[8–10], antiparasitic[11–13], and antiretroviral[14–20] therapies, and also as carriers for cardiovascular therapeutics[21–23]. Erythrocyte carriers are intrinsically biodegradable without the generation of toxic byproducts. They are cleared by macrophages in the reticuloendothelial system of the liver and spleen. As autologous cell-based cargo carriers, RBCs have the advantage of being bio-inert, with no risk of triggering an immune response. Finally, from a practical/translational perspective, they can also be readily manipulated *ex vivo* and stored stably at 4°C.

Despite these attractive properties, the requirement of *ex vivo* manipulation is a significant disadvantage of cell-based therapies in general, because this extra step can be both cumbersome and expensive. Because erythrocytes are non-endocytic and many cargo materials cannot interact with or penetrate their plasma membranes, techniques of cargo encapsulation in RBCs typically rely on mechanisms of membrane perturbation that force cargo molecules into the cell cytosol. Hypotonic treatments have often been used to encapsulate cargoes into erythrocytes.[24–27] Electroporation is

Nanoscale Accepted Manuscript

another widely used technique, particularly for large molecular weight or highly charged cargoes that cannot passively transit the membrane.[28–30] As an alternative to cargo encapsulation within a cell, there are also studies in which cargo molecules have been bound covalently to erythrocyte membranes. Using this technique, erythrocytes have specifically served to deliver vaccine antigens, with delivery of HIV-1 TAT protein being a key example.[31,32]

Gold nanoparticles with organic ligand shells are being explored as candidate drug delivery agents that can carry drugs sequestered within their organic layer, bound reversibly to the gold core, or anchored to the ligand shell.[33–36] Motivated by the potential for such inorganic/organic hybrid nanomaterials to carry therapeutics, here we characterized water-soluble amphiphilic nanoparticles that partition into erythrocyte membranes without the need for membrane perturbation or manipulation, which we hypothesize could be loaded with drugs for direct association with erythrocytes. Using a one-step reaction, we synthesized small ~2-4 nm core size gold nanoparticles (amph-AuNPs) with an amphiphilic ligand shell comprised of two alkanethiols.[37] Each amph-AuNP was coated by a mixture of long-chain mercaptoundecanesulfonate (MUS), an eleven-carbon ligand terminated by a water-soluble sulfonate group, and short-chain hydrophobic octanethiol (OT, **Fig. 1a**). Our previous studies have shown that MUS:OT amph-AuNPs can enter a variety of cells under conditions in which endocytosis has been blocked.[38–41] We have also shown that they can carry oligonucleotide cargos into tumor cells under these conditions.[42] Notably, particle entry into cells was observed without any experimental evidence of membrane poration or disruption. These studies suggest that amph-AuNPs can enter cells passively, likely via a membrane interaction,

Nanoscale Accepted Manuscript

insertion, and/or penetration mechanism, which might be applied to load cells with gold particles in a variety of contexts.

Several studies have shown that AuNPs coated with a hydrophobic ligand shell can interact with and directly embed within synthetic lipid bilayers.[43–47] The basic mechanism put forth in these studies is that the hydrophobic surface ligands of the particles are able to closely associate with the hydrophobic interior of lipid bilayers, enabling stable particle embedding within membranes. However, many of these studies use entirely hydrophobic AuNPs that are insoluble in water and, as a result, require the use of organic solvents to drive AuNP-membrane interactions. A unique property of amph-AuNPs is their environment-sensitive chemistry; in water the sulfonate endgroups of the ligand shell impart solubility, while ligand flexibility enables the hydrophobic octanethiol groups to be exposed during lipid membrane interactions. The water solubility of amphAuNPs is essential for their potential application for direct loading of cell membranes *in vivo*. We have shown in previous work that the presence of 30-60% charged MUS ligand on amph-AuNPs imparts water solubility and their anionic charge does not inhibit high entry into dendiritic cell or fibroblast membranes.[38] Further, we expect that charge-charge repulsion effects between amph-AuNPs and lipid headgroups are mitigated by screening at physiological salt concentrations.

Previously, we tested the uptake of amph-AuNPs by RBCs following brief incubations (1 hr) at relatively low particle concentrations (0.1 mg/mL), and were unable to detect particle interactions with erythrocyte membranes.[49] These results in fact prompted us to develop an assay using RBCs to detect free dye in labeled nanoparticle preparations, since under these conditions free dye would immediately be absorbed into

Nanoscale Accepted Manuscript

the red cell membranes while particle-bound dye remained in solution.[49] However, in very recent work, computational modeling in parallel with experimental studies using model membranes suggested that these amph-AuNPs are not just membrane-penetrating but actually thermodynamically prefer a membrane-embedded state, where the hydrophilic sulfonate headgroups in the amph-AuNP ligand shell 'snorkel' to the aqueous/lipid interface much like transmembrane proteins to achieve a state where free energy is minimized.[48] These studies further suggested that amph-AuNP embedding in membranes is governed by NP core size and surface ligand composition (e.g., hydrophobicity). These findings prompted us to revisit the potential for interactions of amph-AuNPs with RBCs, exploring in more detail particle localization relative to the erythrocyte membrane as a function of NP concentration and time, and the effect of membrane composition itself on NP-membrane interactions.

In this paper, we first present evidence, using multiple analysis techniques, of erythrocyte membrane-embedding by MUS:OT AuNPs and characterize components of the erythrocyte membrane that influence particle insertion. Using the results from this work, we then utilized well-defined giant multilamellar vesicles as model membranes to provide greater insight into the role of membrane composition on particle insertion. The results from this work inform the engineering of these amphiphilic, membrane-embedding gold nanoparticles as potential drug carriers that might associate with erythrocytes *in vivo*, without the need for preliminary *ex vivo* manipulation.

Results & Discussion

Nanoscale Accepted Manuscript

In previous work where we incubated amphiphilic MUS:OT NPs with a 2:1 MUS:OT ligand ratio for 1 hour with erythrocytes, we detected no apparent interaction of the particles with the cells.[49] However, our recent combined experimental and computational studies showed that particles with this composition and a gold core mean diameter of ~2.3 avidly embed within model liposomal membranes to substantial levels,[48] and thus we revisited this experimental setting to determine if RBCs have a particular surface structure that prevents NP embedding or alternatively, if our lack of detecting particle uptake were specific to the particular treatment conditions tested. A key difference in the present study compared to our previously published work[49] is that here, as in our recent model membrane experiments[48], cells were incubated with particles for indicated times and immediately imaged live without further manipulation. In contrast, in our earlier work using RBCs as a 'free dye sensor', cells were washed thoroughly at least three times before analysis.[49] Given our current understanding that amph-AuNPs passively, reversibly, and fluidly insert into membranes, it is reasonable to expect that repeated centrifugation and buffer exchange due to multiple washings might extract membrane-embedded amph-AuNPs back into solution. In the present study, unless cells were fixed first (as for electron microscopy), cells were not washed to remove excess amph-AuNPs after incubation. For these experiments, particles were incubated with cells in PBS (for short-term assays 1-3 hr) or complete medium (RPMI supplemented with the RBC-specific serum replacement Albumax, for long-term assays > 3 hr). We observed no significant differences in amph-AuNP interactions with RBC membranes when comparing uptake in these two treatment conditions. This result is consistent with our previous measurements, which showed that amph-NPs are highly

Nanoscale Accepted Manuscript

resistant to protein adsorption; dynamic light scattering (DLS), TEM, and zeta potential analysis all confirmed that there were no changes in amph-AuNP size or charge when incubated in medium with and without serum.[38]

We prepared 2:1 MUS:OT amph-AuNPs 2.3 ± 1.0 (st. dev.) nm in diameter (batch A, **Fig. 1a, SI Fig. 1a & SI Table 1**) labeled with an alkanethiol-BODIPY fluorescent dye by a place exchange reaction to track the particles' interactions with cells as previously described.[49] When human erythrocytes were co-incubated with the membrane-impermeable dye calcein and BODIPY-labeled amph-AuNPs at 37°C for 3 hours, confocal micrographs showed that calcein remained extracellular, but the gold particles distinctly associated with the plasma membranes of the cells (**Fig. 1b**). This particle signal was low but clearly detectable, and appeared confined to the plasma membrane of the RBCs. Lack of calcein entry into the RBCs indicates that particle binding to the cells was not associated with membrane disruption. Analysis of MUS:OT-treated erythrocytes by flow cytometry at 4°C, 22°C, and 37°C, showed clear temperature-dependent binding, which was highest at 37°C (9-fold compared to untreated cells, **Fig. 1c-d**). Analysis of the kinetics of amph-AuNP binding to RBCs showed that MUS:OT AuNPs (batch B with core size of 2.4 ± 0.8 nm, **SI Fig. 1b & SI Table 1**) associated with erythrocytes as quickly as 5 min at 37°C, with particle uptake increasing rapidly over the first 3 hours and continuing over 24 hr albeit more gradually (**Fig. 1e**). To assay for the stability of amph-AuNP incorporation into RBC membranes, we compared amph-AuNP signal associated with cells after serial washing steps (**SI Fig. 2**). Signal decreased by ~30% after one washing step in PBS and did not

Nanoscale Accepted Manuscript

statistically decrease further after three washes. Even after washing, however, amph-AuNP signal remained significantly above background.

We next compared the behavior of these anionic amph-AuNPs to the interaction of amphiphilic gold nanoparticles bearing a cationic charge. Cationic amph-AuNPs coated with eleven-carbon alkanethiol ligands terminated by trimethylamine (TMA) groups were prepared with a gold core diameter of 5.7 ± 1.5 nm. In clear contrast to the sulfonate-functionalized amph-AuNPs (**Fig. 1b**), BODIPY-labeled TMA AuNPs aggregated significantly on and around erythrocytes, reminiscent of the aggregation reported by Li and Malmstadt for cationic particles that bind to and then extract protrusions of membrane lipids in contact with giant lipid vesicles (**SI Fig. 23**).[50] In addition, incubation with TMA amph-AuNPs led to calcein leakage into many cells (**SI Fig. 2** arrows), indicating that the cationic nanoparticles induced membrane poration. Since TMA particles are known to disrupt cell membranes by virtue of their cationic charge[51,52], it is likely that their charge and not their larger size was responsible for RBC membrane poration. In our previous work, we observed similar membrane disruption in dendritic cells treated with TMA particles of core sizes similar to amph-AuNPs.[38]

The confocal analysis indicated that MUS:OT NPs appear to prefer a membrane-associated state and, since erythrocytes lack a nucleus or internal membranes, it is noteworthy that amph-AuNPs outlined the only cellular membrane present, the plasma membrane. To confirm these observations at the light microcopy level and rule out potential effects of the dye itself, we treated erythrocytes with unlabeled 1:1 MUS:OT NPs of a 2.1 ± 0.8 nm core size (batch C, **SI Fig. 1c & SI Table 1**) for either 1 hr or 16 hr at 37°C, then fixed, embedded, and sectioned them for electron microscopy (**Fig. 2**).

Nanoscale Accepted Manuscript

At both time points, AuNPs were distinctly found associated with the cell surfaces, either directly opposed to the membrane or apparently embedded within it (**Fig. 2a, b**). Distinctly, no particles were found in the cytosol for either time point (**Fig. 2c**). Further, at the highest resolution that we could achieve, it appeared that most of the MUS:OT NPs that decorated the membrane were embedded within it.

Given this confirmation that amph-AuNPs associate with RBCs, we next sought to determine the features of the cell surface that play a role in mediating AuNP-membrane interaction. Since erythrocytes are non-nucleated and free of other organelles, their plasma membrane has a key role in regulating both the structure and function of the entire cell. The erythrocyte membrane, which has been very well studied[53,54], is made up of three components (**Fig. 3**). First, there is a dense glycocalyx on the external face, composed of the polysaccharide chains of glycolipids and glycoproteins capped by sialic acid molecules, which contribute to an overall negative charge. They are the first point of contact with other cells and any interacting nanomaterials. Second, the lipid bilayer of the membrane itself is composed of lipids and cholesterol and also up to 50% by mass of proteins, many of which have transmembrane domains. Third and finally, the spectrin-actin network of the underlying cytoskeleton is intimately and strongly associated with the membrane, creating a tension that controls an erythrocyte's unique mechanical properties that allow it to travel through the myriad vessels of the body's circulatory system. We sought to characterize the role of each of these three contributors to RBC surface properties in turn by treating RBCs with enzymes or inhibitors to remove or alter the function of different membrane components. For each condition, after enzymatic or drug treatment (**Fig. 3**), treatment

Nanoscale Accepted Manuscript

medium was removed, and cells were then incubated with BODIPY-labeled 2:1 MUS:OT NPs (batch B, 2.4 nm core size) for 1-2 hr before analysis of particle association with the cells by flow cytometry.

To study the effect of the glycocalyx on MUS:OT interactions with the membrane, erythrocytes were treated either with neuraminidase to selectively remove only the sialic acids, or with a combination of neuraminidase, heparinase, and hyaluronidase to remove the entire sugar layer on the surface of the cells.[55,56] When sialic acids were preferentially stripped, MUS:OT interactions increased significantly (2.2-fold) compared to unaltered cells treated with AuNPs, suggesting that the interaction of the anionic particles with the RBC membrane is substantially inhibited by these negatively-charged sugars (**Fig. 4a**). When the entire glycocalyx was removed, MUS:OT-membrane interaction increased only slightly further (2.6-fold compared to unaltered cells) (**Fig. 4a**), suggesting that the repulsive negative charge (contributed by the sialic acids) likely plays a bigger role in modulating AuNP-membrane interactions than steric effects contributed by the entire glycocalyx sugar brush. We also stripped the glycocalyx of erythrocytes, held them at 37°C, and treated them for 50 min with unlabeled 1:1 MUS:OT AuNPs with a 2.1 nm core (batch C), and then fixed and prepared them for electron microscopy. As shown in **Fig. 4d**, in agreement with the flow cytometry analysis, amph-AuNPs showed high density embedding in glycocalyx-stripped erythrocyte membranes. Notably, even with the glycocalyx stripped, the electron micrographs showed that all NPs found were apparently membrane-associated and none were found in the cytosol of cells. When erythrocytes were treated with trypsin and chymotrypsin to remove membrane glycoproteins (chiefly of the glycophorin

Nanoscale Accepted Manuscript

family[55–57]), there was no significant difference in AuNP-membrane interaction following this treatment (**Fig. 4b**). Collectively, these results suggest that the cell surface association observed by confocal and electron microscopy reflects favorable particle interactions with the cell membrane itself rather than with cell surface proteins or components of the glycocalyx.

We next tested the role of cytoskeletal-membrane tension on MUS:OT particle interactions with the RBC membrane, by treating RBCs with iodoacetamide and inosine to deplete ATP and thus increase cytoskeletal-membrane tension, or by treating the cells with calyculin A and phorbol 12-myristate 13-acetate (PMA) to activate protein kinase C (PKC), disrupt the spectrin-actin network, and decrease this tension.[58,59] There was no difference in particle association by cells when ATP was depleted to increase tension, but association increased by 1.6-fold when the spectrin-actin network was disrupted to decrease tension (**Fig. 4c**). Since the drugs for this latter treatment were introduced in DMSO, we also treated cells with amph-AuNPs in the presence of the same concentration of DMSO (1 vol%) alone, and saw no effect of the vehicle alone (data not shown). Thus, amph-AuNPs may prefer bilayer areas where cytoskeletal-membrane tension is low.

These experiments with erythrocytes indicated that the surface glycocalyx and charge play significant roles in amph-AuNP/membrane interactions, but the living cell has a highly complex surface structure where many components may simultaneously participate in governing the outcome of nanoparticle binding. Thus, we next moved to a synthetic system of model membranes to better understand and confirm the roles of specific cell surface lipids and sugars on amph-AuNP/membrane association. We

Nanoscale Accepted Manuscript

prepared giant multilamellar vesicles (GMVs) composed of synthetic lipids by gentle hydration.[48] The composition of the erythrocyte membrane has been widely studied and its outer leaflet is composed of phospholipids (glycerophospholipids and sphingomyelin), glycosphingolipids (making up the glycocalyx), and cholesterol.[60,61] GMVs were prepared with a composition of 30.5% phosphatidylcholine (DOPC), 27% sphingomyelin (SM), 25% cholesterol, 7% phosphatydilethanolamine (DOPE), and 10% ganglioside GM1, mimicking the outer leaflet of the RBC membrane[60–62] (**Fig. 5a**). 0.5 mol% 7-nitro-2-1,3-benzoxadiazol-4-yl (NBD)-DOPE was also included as a fluorescent tag for the membranes. GM1, which makes up part of the glycocalyx, has one sugar branch terminated by a sialic acid, and SM has a high melting temperature (T_m) of 37-41°C[63,64]. BODIPY-labeled 2:1 MUS:OT amph-AuNPs with a 2.4 nm core (batch B) were incubated with these RBC-mimic GMVs or control fluorescently-tagged DOPC-only GMVs for 1 hr at room temperature and then imaged by confocal microscopy. We previously showed by confocal microscopy that amph-AuNPs absorb spontaneously into DOPC GMVs, with particles penetrating throughout multilamellar vesicles;[48] this result was again observed here with labeled DOPC GMVs (**Fig. 5b**). By contrast, consistent with the low levels of particle uptake observed for native RBCs at this particle dose and temperature (**Fig. 1c-d**), little or no embedding of amph-AuNPs in erythrocyte outer leaflet mimic GMVs was observed (**Fig. 5b**).

To determine which component(s) of the RBC mimic bilayers were critical for inhibiting particle embedding/penetration relative to simple DOPC membranes, we incrementally added one outer leaflet lipid at a time to DOPC GMVs and measured AuNP uptake by flow cytometry. Compared to the all-DOPC GMVs, AuNP-membrane

Nanoscale Accepted Manuscript

interactions decreased 34% when cholesterol was added, but further addition of DOPE or sphingomyelin had little further impact on particle absorption by the GMVs (BODIPY-labeled 2:1 MUS:OT NPs from batch B, **Fig. 5c**). However, upon introduction of the ganglioside lipid GM1, there was an additional substantial drop in AuNP uptake, giving in total a 92% decrease in AuNP absorption compared with DOPC GMVs. We next prepared a series of seven GMV formulations with pairwise combinations of individual RBC membrane components added in their natural proportion: all DOPC, DOPC/15% DOPE, DOPC/25% cholesterol, DOPC/16% SM, DOPC/10% GM1. GMVs were incubated for 1 hr with BODIPY-labeled 2:1 MUS:OT NPs (batch B, **Fig. 5d**). Compared to the DOPC GMVs, there were decreases in AuNP-membrane interaction in the cases of high T_m SM and negatively-charged GM1. However, this decrease in signal was significant only in the case of GM1, where interaction decreased by 65% compared to the all-DOPC formulation. These results further support our conclusions that the glycocalyx has a central role in modulation of AuNP-membrane interactions.

Finally, to assess the effect of temperature on these interactions, we compared amph-AuNP uptake in sphingomyelin- or GM1-containing GMVs at 22°C and 37°C (**Fig. 5e**). We compared these to all-DOPC GMVs incubated with amph-AuNPs at 22°C as a 'gold standard' for GMVs absorbing high levels of amphiphilic particles. GMVs containing SM but lacking GM1 showed lower particle absorption at 22°C compared to the DOPC control vesicles, but at 37°C, which is at the T_m of SM, amph-AuNP absorption to the membrane-mimic GMVs was comparable to DOPC controls. By contrast, RBC membrane mimics including GM1 showed a substantially lower increase in particle association that increased only 2.4-fold moving from 22°C to 37°C, consistent

Nanoscale Accepted Manuscript

with our whole-cell experiments that suggested the glycocalyx plays an important role in limiting nanoparticle absorption into the cell plasma membrane. Therefore, we conclude that, while increasing temperature to the physiological range overcomes the particle-blocking effect of SM, it has only a small influence on the effect of GM1. These results suggest that while erythrocyte membrane decoration may be wholly sufficient with a glycocalyx intact, perhaps co-administration of neuraminidase (or similar sialic acid-altering molecule) attached to the nanoparticle could be employed to achieve higher levels of NP-membrane interactions.

Conclusions

Employing erythrocytes as 'pharmacytes' – cell-based carriers of therapeutic cargoes – is of great interest, but current techniques first require manipulation of cells *ex vivo* before autologous transfer *in vivo.* Here, we present a system of amphiphilic AuNPs that, by virtue of their core size and surface ligand hydrophobicity, are able to embed within erythrocyte membranes. We have shown that amph-AuNP-membrane embedding depends on membrane fluidity and the glycocalyx, and particle association with RBC membranes is promoted by increasing temperature (up to physiological levels) or when the glycocalyx in general or the sialic acids in particular are removed. Our studies with model lipid membranes further suggest that the high T_m lipid SM plays a key role in modulating amph-AuNP association with RBC membranes at room temperature but GM1 plays a more important role at physiological temperature. These results inform design characteristics needed to achieve optimal membrane-embedding by amphiphilic nanoparticles. Altogether, these results suggest that these amph-AuNPs

Nanoscale Accepted Manuscript

may be useful as drug carriers that may mediate easy and rapid embedding into erythrocyte membranes *in vivo* without the need for *ex vivo* manipulation.

Experimental

Materials

$HAuCl_4$ salt, OT ligand, and calcein were purchased from Sigma. BODIPY 630/650-X succinimidyl ester was purchased from Invitrogen. MUS ligands were prepared in-house with a method described previously.[38] Amph-AuNPs were also prepared in-house as described previously.[37] Neuraminidase, hyaluronidase, and heparinase were purchased from Sigma, as were trypsin and chymo-trypsin. Calyculin A, phorbol 12-myristate 13-acetate (PMA), iodoacetamide, and inosine were also purchased from Sigma. All lipids and cholesterol were purchased from Avanti Polar Lipids.

AuNP synthesis, characterization, & labeling

We used a modified one-phase Brust-Schiffrin synthesis to prepare amph-AuNPs.[65] Briefly, a solution of $HAuCl_4$ was prepared in ~200 mL ethanol and an equimolar mixture of thiol ligands was prepared in methanol. These two solutions were mixed together and allowed to stir for 15 min. A saturated solution of $NaBH_4$ in ethanol was then added slowly and drop-wise and, following this step, the reaction was allowed to stir for an additional 3 hr. The flask was placed at 4°C overnight after which the precipitated particles were isolated by filtration through qualitative filter paper. The filtered particles were washed sequentially in ethanol and methanol and dried with

Nanoscale Accepted Manuscript

further washes in acetone. Before characterization or analysis, insoluble NPs were first removed by dissolving ~10 mg dry NPs in 1 mL water, centrifuging at 14,000 x g for 2 min, and isolating the soluble NPs that remain in the supernatant. Size distributions of NP batches were determined using transmission electron microscopy (TEM). ImageJ software was used to quantify the sizes of NPs from high magnification TEM images, which were subsequently used to calculate the mass extinction coefficient.

A BODIPY-C11-SH dye construct was prepared in-house by adding an alkylthiol linker to BODIPY 630/650-X, succinimidyl ester. Amph-AuNPs were labeled by place-exchange of BODIPY-C11-SH with surface ligands by incubating 30 μmoles of dye construct per mg of NPs over 2-4 days at 22°C with constant shaking or stirring. Labeled AuNPs were purified and separated from excess dye by precipitation and washing in acetone at least 5x. Washed amph-AuNPs were dried overnight and solubilized in water for use.

Erythrocyte preparation, enzyme treatment, & incubation with amph-AuNPs

Human erythrocytes were stored in packed volume at 4°C. Prior to use, 200 μL of packed erythrocytes were washed 3x in 1 mL PBS or complete RPMI with Albumax, and finally resuspended in 1 mL PBS/medium for use. To prepare experimental samples, 2-4 μL of this cell stock (4-8 million cells) were used per sample. Amph-AuNP concentrations of 0.07, 0.14, and 0.28 mg/mL were used for incubation times of 1-3 hr at 4°C, 22°C, and 37°C where necessary. Prior to incubation at given temperatures, erythrocytes were pre-incubated by a ~20-min equilibration to the desired temperature before adding AuNPs. For assaying uptake kinetics, erythrocytes were incubated at

Nanoscale Accepted Manuscript

0.07 mg/mL at 37°C with continuous rotation. Fluorescence was analyzed by flow cytometry without washing of excess AuNPs at 5 min, 30 min, 1 hr, 3 hr, and 24 hr. All erythrocytes were obtained with approval by and in accordance with MIT guidelines.

Stripping of sialic acids & glycocalyx

To selectively strip the sialic acids off the surface of the membrane, erythrocytes were treated with neuraminidase at 0.1 U/mL for 2 hr at 22°C with continuous rotation. To strip the entire glycocalyx off the surface of the membrane, erythrocytes were treated with a combination of neuraminidase at 0.1 U/mL, heparinase at 5 U/mL, and hyaluronidase at 50 μg/mL for 2 hr at 22°C with continuous rotation. After treatment, cells were pelleted, excess enzymes were removed, and amph-AuNPs were added.

Removal of membrane proteins

To remove membrane glycoproteins, erythrocytes were co-treated with trypsin and chymo-trypsin at 1 mg/mL each at 22°C with continuous rotation. After treatment, cells were pelleted, excess enzymes were removed, and amph-AuNPs were added.

Increasing/decreasing cytoskeletal-membrane tension

To deplete ATP and increase cytoskeletal-membrane tension, erythrocytes were treated with a medium of 6 mM iodoacetamine and 10 mM inosine in PBS without glucose for 3 hr at 22°C with continuous rotation. After treatment, cells were pelleted, and initial treatment volumes were removed. Amph-AuNPs were then added in the same ATP depletion buffer.

Nanoscale Accepted Manuscript

To disrupt spectrin/actin networks and decrease cytoskeletal-membrane tension, erythroctyes were treated first with 0.2 μM calyculin A for 30 min at 22°C. Following this incubation, cells were pelleted, treatment medium was removed, and PMA was added for 90 min also at 22°C. Samples were rotated continuously during these incubations. Finally, cells were pelleted, treatment volumes were removed, and amph-AuNPs were added.

GMV synthesis & preparation

To synthesize GMVs, lipid stocks in chloroform were added to glass scintillation vials, where total lipid was 1 μmole per vial. When fluorescent lipid tracers were necessary to label GMVs, dyes were added at 0.1-0.5 mol%. Chloroform was allowed to evaporate overnight at 22°C, in order to form lipid films on glass. Uncapped vials were then incubated in a water bath at 70°C for > 6 hr, and this step allowed these films to hydrate without immersion in solution. Sucrose buffer (50 mM in water or PBS) was then added at 2 mL per vial, and vials were capped and further incubated at 70°C overnight, allowing GMVs to form. GMVs were gently harvested with minimal agitation or mixing the following day, after first cooling to 22°C.

For the outer leaflet set (**Fig. 4c**), the following formulations were used: 1) all-DOPC, 2) 75% DOPC/25% cholesterol, 3) 68% DOPC/7% DOPE/25% cholesterol, 4) 41% DOPC/7% DOPE/25% cholesterol/27% SM, and 5) 31% DOPC/27% SM/7% DOPE /25% cholesterol/10% GM1. For the pair-wise GMV set (**Fig. 4d**), the following

Nanoscale Accepted Manuscript

formulations were used: 1) all DOPC, 2) DOPC/15% DOPE, 3) DOPC/25% cholesterol, 4) DOPC/16% SM, and 5) DOPC/10% GM1.

Confocal microscopy

For erythrocytes, 4 million cells were added to 200 µL per well of an 8-well LabTek chamber (Nunc). Calcein was added at 20 µg/mL and BODIPY-MUS:OT 2:1 amph-AuNPs were added at 0.28 mg/mL. Treatment medium was prepared before the addition of cells and samples were rocked back and forth gently without mixing or agitation with a pipette. Samples were imaged with a LSM 510 confocal microscope (Carl Zeiss). Z-stacks were collected using an optical slice thickness of 1 µm, and images were analyzed with Zeiss LSM software.

For GMVs, confocal samples were prepared in 8-well LabTek chambers (Nunc) and, prior to adding GMVs, we first prepared solutions of 50 mM glucose in water with BODIPY-MUS:OT 2:1 amph-AuNPs at 0.07 mg/mL. GMV harvests in sucrose were mixed 1-2x with a pipette and added at a 1:4 ratio in a sample well. Notably, samples were only rocked back and forth after preparation and there was no additional mixing of GMVs with AuNPs in the well. Samples were incubated 1-3 hr at 22°C, unless otherwise noted. Samples were then imaged with a LSM 510 confocal microscope (Carl Zeiss). Z-stacks were collected using an optical slice thickness of 1 µm, and images were analyzed with Zeiss LSM software.

Flow cytometry

Nanoscale Accepted Manuscript

For erythrocytes, 4-8 million cells were added per 200 µL per round-bottom sample tube and either treated first with membrane-perturbing enzymes (as described above) or with BODIPY-labeled MUS:OT 2:1 amph-AuNPs at 0.07, 0.14, or 0.28 mg/mL for 1 hr. Tubes were rotated continuously at a desired incubation temperature. Samples from tubes were transferred to 96-well round-bottom plates (BD) or polystyrene flow cytometry tubes (BD Falcon) for analysis. Samples were analyzed with a LSR Fortessa HTS flow cytometer (BD) and data were analyzed using FlowJo software.

For GMVs, flow cytometry samples were prepared in 96-well round-bottom plates (BD) or polystyrene flow cytometry tubes (BD Falcon). We first prepared solutions of 50 mM sucrose in water with BODIPY-MUS:OT 2:1 amph-AuNPs at 0.07 mg/mL in sample wells. GMV harvests in sucrose were mixed 1-2x with a pipette and added at a 1:1.5 ratio per sample well. Samples were rocked gently back and forth after preparation – but there was no additional mixing of GMVs with AuNPs in the wells. Samples were incubated at 1-3 hr and 22°C, unless otherwise noted. Samples were then analyzed with a LSR Fortessa HTS flow cytometer (BD) and data were analyzed using FlowJo software.

Cell electron microscopy

For cell EM, cell fixative was first prepared as 2.5% gluteraldehyde, 3% paraformaldehyde with 5% sucrose in 0.1M sodium cacodylate buffer (pH 7.4). Since erythrocytes are in suspension, 200 µL of fixative was added to 200 µL sample volume, rotated for 1 min at incubation temperature of 37°C, pelleted, and resuspended in 1 mL

Nanoscale Accepted Manuscript

fixative. After fixing, cells were pelletted, and post-fixed in 1% OsO_4 in veronal-acetate buffer. The cell pellet was stained in block overnight with 0.5% uranyl acetate in veronal-acetate buffer (pH 6.0), then dehydrated and embedded in Embed-812 resin. Sections were cut on a Reichert Ultracut E microtome with a Diatome diamond knife at a thickness setting of 50 nm. The sections were examined using a FEI Tecnai Spirit at 80KV and photographed with an AMT CCD camera.

Nanoscale Accepted Manuscript

Acknowledgements

We would like to acknowledge Jeff Wagner, Jim Abshire, and Jacquin Niles for providing erythrocytes. This work was supported by the U. S. Army Research Laboratory and the U. S. Army Research Office through the Institute for Soldier Nanotechnologies, under contract number W911NF-13-D-0001.

Nanoscale Accepted Manuscript

References

1. Hamidi, M., Zarrin, A., Foroozesh, M. & Mohammadi-Samani, S. Applications of carrier erythrocytes in delivery of biopharmaceuticals. *J. Controlled Release* **118,** 145–160 (2007).
2. Pierigè, F., Serafini, S., Rossi, L. & Magnani, M. Cell-based drug delivery. *Adv. Drug Deliv. Rev.* **60,** 286–295 (2008).
3. Eichler, H. G., Raffesberg, W., Gasic, S., Korn, A. & Bauer, K. Release of vitamin B12 from carrier erythrocytes in vitro. *Res. Exp. Med. (Berl.)* **185,** 341–344 (1985).
4. Pitt, E., Lewis, D. A. & Offord, R. E. The use of corticosteroids encapsulated in erythrocytes in the treatment of adjuvant induced arthritis in the rat. *Biochem. Pharmacol.* **32,** 3355–3358 (1983).
5. Rossi, L. *et al.* Erythrocyte-mediated delivery of dexamethasone in patients with chronic obstructive pulmonary disease. *Biotechnol. Appl. Biochem.* **33,** 85–89 (2001).
6. Rossi, L. *et al.* Low doses of dexamethasone constantly delivered by autologous erythrocytes slow the progression of lung disease in cystic fibrosis patients. *Blood Cells. Mol. Dis.* **33,** 57–63 (2004).
7. Annese, V. *et al.* Erythrocytes-Mediated Delivery of Dexamethasone in Steroid-Dependent IBD Patients—A Pilot Uncontrolled Study. *Am. J. Gastroenterol.* **100,** 1370–1375 (2005).
8. Updike, S. J., Wakamiya, R. T. & Lightfoot, E. N. Asparaginase entrapped in red blood cells: action and survival. *Science* **193,** 681–683 (1976).
9. Alpar, H. O. & Lewis, D. A. Therapeutic efficacy of asparaginase encapsulated in intact erythrocytes. *Biochem. Pharmacol.* **34,** 257–261 (1985).

Nanoscale Accepted Manuscript

10. Jr, D. & C, B. Circulating carrier erythrocytes: slow-release vehicle for an antileukemic drug, cytosine arabinoside. *Am. J. Vet. Res.* **43,** 2210–2212 (1982).

11. Talwar, N. & Jain, N. K. Erythrocytes as carriers of primaquine-preparation: characterization and evaluation. *J. Controlled Release* **20,** 133–141 (1992).

12. Talwar, N. & Jain, N. K. Erythrocytes as carriers of metronidazole: In-vitro characterization. *Drug Dev. Ind. Pharm.* **18,** 1799–1812 (1992).

13. Berman, J. D. & Gallalee, J. V. Antileishmanial Activity of Human Red Blood Cells Containing Formycin A. *J. Infect. Dis.* **151,** 698–703 (1985).

14. Rossi, L. *et al.* Erythrocyte-mediated delivery of a new homodinucleotide active against human immunodeficiency virus and herpes simplex virus. *J. Antimicrob. Chemother.* **47,** 819–827 (2001).

15. Perno, C.-F. *et al.* Red blood cells mediated delivery of 9-(2-phosphonylmethoxyethyl)adenine to primary macrophages: efficiency, metabolism and activity against human immunodeficiency virus or herpes simplex virus. *Antiviral Res.* **33,** 153–164 (1997).

16. Fraternale, A. *et al.* Macrophage protection by addition of glutathione (GSH)-loaded erythrocytes to AZT and DDI in a murine AIDS model. *Antiviral Res.* **56,** 263–272 (2002).

17. Fraternale, A. *et al.* New drug combinations for the treatment of murine AIDS and macrophage protection. *Eur. J. Clin. Invest.* **31,** 248–252 (2001).

18. Fraternale, A. *et al.* Erythrocytes as carriers of reduced glutathione (GSH) in the treatment of retroviral infections. *J. Antimicrob. Chemother.* **52,** 551–554 (2003).

Nanoscale Accepted Manuscript

19. Rossi, L. *et al.* Heterodimer-Loaded Erythrocytes as Bioreactors for Slow Delivery of the Antiviral Drug Azidothymidine and the Antimycobacterial Drug Ethambutol. *AIDS Res. Hum. Retroviruses* **15,** 345–353 (1999).

20. Magnani, M. *et al.* FIV infection of macrophages: in vitro and in vivo inhibition by dideoxycytidine 5′-triphosphate. *Vet. Immunol. Immunopathol.* **46,** 151–158 (1995).

21. Tajerzadeh, H. & Hamidi, M. Evaluation of Hypotonic Preswelling Method for Encapsulation of Enalaprilat in Intact Human Erythrocytes. (2000). at <http://informahealthcare.com/doi/abs/10.1081/DDC-100102306>

22. Hamidi, M., Tajerzadeh, H., Dehpour, A.-R. & Ejtemaee-Mehr, S. Inhibition of serum angiotensin-converting enzyme in rabbits after intravenous administration of enalaprilat-loaded intact erythrocytes. *J. Pharm. Pharmacol.* **53,** 1281–1286 (2001).

23. Hamidi, M., Tajerzadeh, H., Dehpour, A.-R., Rouini, M.-R. & Ejtemaee-Mehr, S. In Vitro Characterization of Human Intact Erythrocytes Loaded by Enalaprilat. (2008). at <http://informahealthcare.com/doi/abs/10.1080/107175401317245903>

24. Ihler, G. M. & Tsang, H. C. Hypotonic hemolysis methods for entrapment of agents in resealed erythrocytes. *Methods Enzymol.* **149,** 221–229 (1987).

25. Pitt, E., Johnson, C. M., Lewis, D. A., Jenner, D. A. & Offord, R. E. Encapsulation of drugs in intact erythrocytes: An intravenous delivery system. *Biochem. Pharmacol.* **32,** 3359–3368 (1983).

26. Adriaenssens, K., Karcher, D., Lowenthal, A. & Terheggen, H. G. Use of enzyme-loaded erythrocytes in in-vitro correction of arginase-deficient erythrocytes in familial hyperargininemia. *Clin. Chem.* **22,** 323–326 (1976).

Nanoscale Accepted Manuscript

27. Ihler, G. M., Glew, R. H. & Schnure, F. W. Enzyme Loading of Erythrocytes. *Proc. Natl. Acad. Sci.* **70,** 2663–2666 (1973).

28. Kinosita, K. & Tsong, T. Y. Survival of sucrose-loaded erythrocytes in the circulation. *Nature* **272,** 258–260 (1978).

29. Zimmermann, U., Riemann, F. & Pilwat, G. Enzyme loading of electrically homogeneous human red blood cell ghosts prepared by dielectric breakdown. *Biochim. Biophys. Acta BBA - Biomembr.* **436,** 460–474 (1976).

30. Mitchell, D., James, G. & Kruse, C. Bioactivity of electric field-pulsed human recombinant interleukin-2 and its encapsulation into erythrocyte carriers. *Biotechnol. Appl. Biochem.* **12,** 264–275 (1990).

31. Corinti, S. *et al.* Erythrocytes deliver Tat to interferon-γ-treated human dendritic cells for efficient initiation of specific type 1 immune responses in vitro. *J. Leukoc. Biol.* **71,** 652–658 (2002).

32. Dominici, S. *et al.* Red blood cell-mediated delivery of recombinant HIV-1 Tat protein in mice induces anti-Tat neutralizing antibodies and CTL. *Vaccine* **21,** 2073–2081 (2003).

33. Giljohann, D. A. *et al.* Gold Nanoparticles for Biology and Medicine. *Angew. Chem. Int. Ed.* **49,** 3280–3294 (2010).

34. Tiwari, P. M., Vig, K., Dennis, V. A. & Singh, S. R. Functionalized Gold Nanoparticles and Their Biomedical Applications. *Nanomaterials* **1,** 31–63 (2011).

35. Ding, Y. *et al.* Gold Nanoparticles for Nucleic Acid Delivery. *Mol. Ther.* **22,** 1075–1083 (2014).

Nanoscale Accepted Manuscript

36. Dreaden, E. C., Alkilany, A. M., Huang, X., Murphy, C. J. & El-Sayed, M. A. The golden age: gold nanoparticles for biomedicine. *Chem. Soc. Rev.* **41,** 2740–2779 (2012).

37. Uzun, O. *et al.* Water-soluble amphiphilic gold nanoparticles with structured ligand shells. *Chem. Commun.* 196 (2008). doi:10.1039/b713143g

38. Verma, A. *et al.* Surface-structure-regulated cell-membrane penetration by monolayer-protected nanoparticles. *Nat Mater* **7,** 588–595 (2008).

39. Verma, A. & Stellacci, F. Effect of Surface Properties on Nanoparticle–Cell Interactions. *Small* **6,** 12–21 (2010).

40. Leduc, C., Jung, J.-M., Carney, R. R., Stellacci, F. & Lounis, B. Direct Investigation of Intracellular Presence of Gold Nanoparticles via Photothermal Heterodyne Imaging. *ACS Nano* **5,** 2587–2592 (2011).

41. Carney, R. P., Carney, T. M., Mueller, M. & Stellacci, F. Dynamic Cellular Uptake of Mixed-Monolayer Protected Nanoparticles. *Biointerphases* **7,** 17 (2012).

42. Jewell, C. M. *et al.* Oligonucleotide Delivery by Cell-Penetrating 'Striped' Nanoparticles. *Angew. Chem.* **123,** 12520–12523 (2011).

43. Rasch, M. R. *et al.* Hydrophobic Gold Nanoparticle Self-Assembly with Phosphatidylcholine Lipid: Membrane-Loaded and Janus Vesicles. *Nano Lett* **10,** 3733–3739 (2010).

44. Rasch, M. R., Yu, Y., Bosoy, C., Goodfellow, B. W. & Korgel, B. A. Chloroform-Enhanced Incorporation of Hydrophobic Gold Nanocrystals into Dioleoylphosphatidylcholine (DOPC) Vesicle Membranes. *Langmuir* **28,** 12971–12981 (2012).

Nanoscale Accepted Manuscript

45. An, X., Zhan, F. & Zhu, Y. Smart Photothermal-Triggered Bilayer Phase Transition in AuNPs–Liposomes to Release Drug. *Langmuir* **29,** 1061–1068 (2013).

46. Tatur, S., Maccarini, M., Barker, R., Nelson, A. & Fragneto, G. Effect of Functionalized Gold Nanoparticles on Floating Lipid Bilayers. *Langmuir* **29,** 6606–6614 (2013).

47. Park, S.-H., Oh, S.-G., Mun, J.-Y. & Han, S.-S. Loading of gold nanoparticles inside the DPPC bilayers of liposome and their effects on membrane fluidities. *Colloids Surf. B Biointerfaces* **48,** 112–118 (2006).

48. Van Lehn, R. C. *et al.* Effect of Particle Diameter and Surface Composition on the Spontaneous Fusion of Monolayer-Protected Gold Nanoparticles with Lipid Bilayers. *Nano Lett.* **13,** 4060–4067 (2013).

49. Andreozzi, P., Martinelli, C., Carney, R. P., Carney, T. M. & Stellacci, F. Erythrocyte Incubation as a Method for Free-Dye Presence Determination in Fluorescently Labeled Nanoparticles. *Mol. Pharm.* **10,** 875–882 (2013).

50. Li, S. & Malmstadt, N. Deformation and poration of lipid bilayer membranes by cationic nanoparticles. *Soft Matter* **9,** 4969 (2013).

51. Leroueil, P. R. *et al.* Wide Varieties of Cationic Nanoparticles Induce Defects in Supported Lipid Bilayers. *Nano Lett.* **8,** 420–424 (2008).

52. Leroueil, P. R. *et al.* Nanoparticle Interaction with Biological Membranes: Does Nanotechnology Present a Janus Face? *Acc. Chem. Res.* **40,** 335–342 (2007).

53. Mohandas, N. & Gallagher, P. G. Red cell membrane: past, present, and future. *Blood* **112,** 3939–3948 (2008).

Nanoscale Accepted Manuscript

54. Mohandas, N. & Evans, E. Mechanical Properties of the Red Cell Membrane in Relation to Molecular Structure and Genetic Defects. *Annu. Rev. Biophys. Biomol. Struct.* **23,** 787–818 (1994).

55. Ganguly, K. *et al.* The Glycocalyx Protects Erythrocyte-Bound Tissue-Type Plasminogen Activator from Enzymatic Inhibition. *J. Pharmacol. Exp. Ther.* **321,** 158–164 (2007).

56. Fritsch, P., Wolff, K. & Hönigsmann, H. Glycocalyx of Epidermal Cells in Vitro: Demonstration and Enzymatic Removal. *J. Invest. Dermatol.* **64,** 30–37 (1975).

57. Duraisingh, M. T., Maier, A. G., Triglia, T. & Cowman, A. F. Erythrocyte-binding antigen 175 mediates invasion in Plasmodium falciparum utilizing sialic acid-dependent and -independent pathways. *Proc. Natl. Acad. Sci.* **100,** 4796–4801 (2003).

58. Betz, T., Lenz, M., Joanny, J.-F. & Sykes, C. ATP-dependent mechanics of red blood cells. *Proc. Natl. Acad. Sci.* **106,** 15320–15325 (2009).

59. Manno, S., Takakuwa, Y. & Mohandas, N. Modulation of Erythrocyte Membrane Mechanical Function by Protein 4.1 Phosphorylation. *J. Biol. Chem.* **280,** 7581–7587 (2005).

60. Qutub, Y., Uzunova, V., Galkin, O. & Vekilov, P. G. Interactions of Hemin with Model Erythrocyte Membranes. *J Phys Chem B* **114,** 4529–4535 (2010).

61. Bernhardt, I. & Ellory, J. C. *Red Cell Membrane Transport in Health and Disease*. (Springer, 2003).

Nanoscale Accepted Manuscript

62. Virtanen, J. A., Cheng, K. H. & Somerharju, P. Phospholipid composition of the mammalian red cell membrane can be rationalized by a superlattice model. *Proc. Natl. Acad. Sci.* **95,** 4964–4969 (1998).

63. Brown, D. A. & London, E. Structure and Function of Sphingolipid- and Cholesterol-rich Membrane Rafts. *J. Biol. Chem.* **275,** 17221–17224 (2000).

64. Veatch, S. L. & Keller, S. L. Miscibility Phase Diagrams of Giant Vesicles Containing Sphingomyelin. *Phys. Rev. Lett.* **94,** 148101 (2005).

65. Brust, M., Walker, M., Bethell, D., Schiffrin, D. J. & Whyman, R. Synthesis of thiol-derivatised gold nanoparticles in a two-phase Liquid?Liquid system. *J. Chem. Soc. Chem. Commun.* 801 (1994). doi:10.1039/c39940000801

Nanoscale Accepted Manuscript

Figure captions

Figure 1. (a) MUS:OT amph-AuNP schematic detailing chemical structures of surface ligands. (b) Human erythrocytes incubated with BODIPY-MUS:OT 2:1 amph-AuNPs at 0.28 mg/mL and calcein at 20 μg/mL for 3 hr at 37°C and imaged with a confocal microscope (scale bars on left panel 50 μm). (c, d) BODIPY-MUS:OT 2:1 NPs at 0.28 mg/mL were incubated with erythrocytes at 4°C, 22°C, and 37°C for 3 hr, and interaction was analyzed by flow cytometry (c), and quantified (error bars for standard error of the mean, SEM; significance noted directly above columns indicates value of that column relative to untreated control) (d). Statistics were performed with a one-way ANOVA test, followed by Tukey's multiple comparison test ($P < 0.05$ is significant, *** indicates $P < 0.0001$). (e) Kinetics of BODIPY-MUS:OT 2:1 AuNPs at 0.07 mg/mL association with erythrocytes over 24 hr at 37°C (error bars for SEM). All experiments were performed with at least 3 biological replicates per condition.

Figure 2. Erythrocytes treated with unlabeled 1:1 MUS:OT amph-AuNPs (batch C) for 16 hr at 37°C were fixed and sectioned for TEM imaging. Scale bars 200 nm for (a) and (b), and 100 nm for (c).

Figure 3. Schematic diagramming erythrocyte membrane components and treatment methods used to perturb them.

Figure 4. (a-c) RBCs were incubated with BODIPY-MUS:OT 2:1 amph-AuNPs (batch B, 0.08 mg/mL) for 1 hr at 22°C and then analyzed for nanoparticle association by flow

Nanoscale Accepted Manuscript

cytometry. (a) RBCs were treated with enzymes removing sialic acids or the entire glycocalyx prior to NP incubation. (b) RBCs were treated with trypsin and chymotrypsin to remove cell surface glycoproteins prior to NP incubation. (c) RBCs were treated with drugs increasing or decreasing membrane tension prior to NP incubation. Statistics were performed with a one-way ANOVA test, followed by Bonferroni's multiple comparison test ($P < 0.05$ is significant, *** indicates $P < 0.0001$). All experiments were performed with at least 3 biological replicates per condition. (d) Cell electron micrograph of unlabeled 1:1 MUS:OT amph-AuNPs (batch C, incubated for 1 hr at 37°C) as they interacted with erythrocytes that had their glycocalyx stripped, scale bar 200 nm.

Figure 5. (a) Synthetic lipids used to make model erythrocyte membranes. (b) Confocal micrographs of all-DOPC GMVs and erythrocyte outer leaflet GMVs treated with BODIPY-MUS:OT 2:1 amph-AuNPs (batch B, 0.07 mg/mL) for 1 hr at 22°C, scale bars 50 μm. (c, d) Amph-AuNPs (batch B, 0.07 mg/mL) were incubated with incremental GMV formulations (c) or GMVs incorporating individual membrane components (d) for 1 hr at 22°C, and analyzed for NP/membrane association by flow cytometry. Median fluorescence intensities of particles associated with GMVs (error bars for SEM between individual sample replicates). In (c), significance noted directly above columns is compared to the DOPC/DOPE/chol/SM/GM1 case. In (d), significance noted directly above columns is compared to the all-DOPC case. (e) Amph-AuNPs (batch B, 0.07 mg/mL) incubated with GMVs with or without GM1 present at 22°C and 37°C and assessed after 1 hr by flow cytometry. Significance noted directly

Nanoscale Accepted Manuscript

above columns is compared to the all-DOPC case (22°C). Statistics were performed with a one-way ANOVA test, followed by Tukey's multiple comparison test ($P < 0.05$ is significant, *** indicates $P < 0.0001$). All experiments were performed with at least 3 biological replicates per condition.

Supplementary information

SI Figure 1. Core size distribution from ImageJ analysis of TEM images of each amph-AuNP batch used with representative TEM images.

SI Figure 2. Erythrocytes treated with BODIPY-MUS:OT 2:1 amph-AuNPs at 0.28 mg/mL for 3 hr at 37°C. Error bars are for standard error of the mean, SEM. Statistics were performed with a one-way ANOVA test, followed by Bonferroni's multiple comparison test ($P < 0.05$ is significant, *** indicates $P < 0.0001$). At least 3 biological replicates were used per condition.

SI Figure 3. Erythrocytes co-treated with calcein at 50 μg/mL and BODIPY-TMA as control NPs. Scale bars 50 μm.

SI Table 1. Mean core size and st. dev. for amph-AuNP batches A-C used in this study.

Nanoscale Accepted Manuscript